# $\eta$ 5 –$\eta$ 1 Switch in Divalent Phosphaytterbocene Complexes with Neutral Iminophosphoranyl Pincer Ligands: Solid-State Structures and Solution NMR 1 J Yb–P Coupling Constants

Thibault Cheisson, Audrey Auffrant, Grégory Nocton

# $\eta^5$-$\eta^1$ Switch in Divalent Phosphaytterbocene Complexes with Neutral Iminophosphoranyl Pincer Ligands: Solid-State Structures and Solution NMR $^1J_{Yb\text{-}P}$ Coupling Constants

Thibault Cheisson,[†] Audrey Auffrant,*[†] and Grégory Nocton*[†]

[†] *Laboratoire de Chimie Moléculaire, CNRS, Ecole Polytechnique, Palaiseau, France.*

*Supporting Information Placeholder*

**ABSTRACT:** This manuscript reports the synthesis of a series of complexes based on the bis(pentamethylcyclopentadienyl)ytterbium(II) (Cp*$_2$Yb) (**1**) and bis(tetramethylphospholyl)ytterbium(II) (Tmp$_2$Yb) (**2**) fragments bearing an additional neutral bis(methyliminophosphoranyl)pyridine ligand (**L**) on which the steric demand was modulated at the phosphorus position (triethyl, $\mathbf{L^{Et}}$; triphenyl, $\mathbf{L^{Ph}}$ and tricyclohexyl, $\mathbf{L^{Cy}}$) to yield the original complexes Cp*$_2$YbL$^{Et}$ (**1-L$^{Et}$**), Cp*$_2$YbL$^{Ph}$ (**1-L$^{Ph}$**), Tmp$_2$YbL$^{Et}$ (**2-L$^{Et}$**), Tmp$_2$YbL$^{Ph}$ (**2-L$^{Ph}$**) and Tmp$_2$YbL$^{Cy}$ (**2-L$^{Cy}$**) while no reaction occurs between **1** and $\mathbf{L^{Cy}}$. The crystal structures of these sterically crowded complexes are reported as well as room temperature NMR data for all the complexes. The solid-state coordination mode of $\mathbf{L^R}$ differs depending on the nature of the fragments **1** and **2** and on the steric bulk of $\mathbf{L^R}$. The crystal structure of the divalent Tmp$_2$Yb(py)$_2$ (**3**) is also reported for structural and spectroscopic comparisons. Interestingly, in both **2-L$^{Et}$** and **2-L$^{Cy}$**, one of the two Tmp ligands coordinates in $\eta^1$ rather than in $\eta^5$, a relevant coordination mode for the study of Sterically Induced Reductions. The behavior of those complexes in solution varies with the sterics and electronics of the ligands as demonstrated by variable temperature NMR experiments. In solution, the $^1J_{Yb\text{-}P}$ coupling is used to track the coordination mode of the Tmp ligand and a large difference of $^1J_{Yb\text{-}P}$ coupling constant allows the distinction between a $\eta^5$- coordination mode and a dynamical $\eta^5$-$\eta^1$switch.

## INTRODUCTION

The chemistry of divalent lanthanide complexes presents multiple interesting facets and their use in organic chemistry or in the activation of small molecules remains an attractive research area.[1,2] In these reactions, the coordination of the small molecule (organic or not) is usually followed by a single electron transfer process, which leads to its mono-electronic reduction and to the oxidation of the metal center to its trivalent state, the most stable oxidation state of lanthanides.[3,4] Once this transfer is achieved, the reduced ligand reacts in different ways and many examples are reported including simple protonation,[5] insertion chemistry,[6] C-C radical coupling (reversible or not),[7-10] C-H activation[11] or a second electron transfer provided by another divalent lanthanide complex to form dimers. The versatility of these reactions reinforces the need of the deep understanding of the coordination chemistry of divalent lanthanides complexes and the study of the surrounding ligand's steric bulk is of particular interest.[12]

For decades, the coordination chemistry of divalent lanthanide complexes have been dominated by cyclopentadienyl ligand with different substituents leading to modifications in the electronic structures of the metal center in agreement with the donation capacity of the substituents.[4] Very recently, other ligands such as silyloxides,[13] silyls[14] or chelate podant ligands[15] appeared in the coordination chemistry of divalent lanthanides complexes leading to drastic modification of their electronics and interesting reactivity with $CO_2$[13] or $CS_2$[15] for example. The modification of the electronic structure in these complexes is not the only way of setting up chemical reactions and the use of a large steric bulk has also been shown to be effective. In 2008, Harder *et al.* reported the spontaneous reduction of a trivalent samarium complex with a bulky Cp$^{BIG}$ ligand,[16] an interesting example of the Sterically Induced Reduction[17] discovered in the end of the 90s by Evans for the Cp*$_3$Sm complex.[18] In the latter complex, the steric bulk around the trivalent samarium complex induced a reduction with a concomitant departure of a radical ligand and very interesting reactivity has been described from this singularity.[17]

Recently, some of us reported the room temperature bipyridine reduction with a concomitant departure of a bulky phospholyl radical ligand at a thulium metal center.[19] The mechanism of this intriguing reaction was investigated and the possibility of an easy $\eta^5$–$\eta^1$ switch of the phospholyl ligand appeared as a good potential explanation to justify the formation of a bisphospholyl bispyridine thulium intermediate complex that triggers the reactivity. The possibility of a $\eta^5$–$\eta^1$ switch of one cyclopentadienyl ligand is also postulated to be the key intermediate to explain the sterically induced reduction.[20] However, there are not many spectroscopic tools known to effectively track these types of $\eta^1$ intermediate in solution. If this coordination mode was reported with rare earth metal ions,[21-28] the Cp ligand is always supported by another different metal ion. To the best of our knowledge, this coordination mode is not yet reported for Cp ligands only supported by lanthanides. The equilibrium and dynamic solution behavior between the two coordination modes usually prevents to trap such intermediates and only few lanthanides complexes have been described by X-ray with such a coordination mode and concern phospholyl complexes of samarium (Chart 1).[29,30]

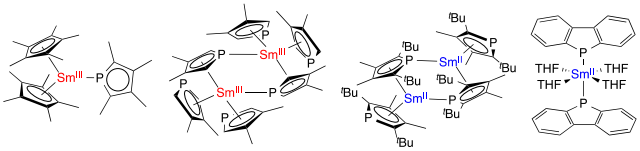

**Chart 1.**

In the present work, we report the coordination chemistry of bis(pentamethylcyclopentadienyl)ytterbium(II) ($Cp^*_2Yb$), **1**, and bis(tetramethylphospholyl)ytterbium(II) ($Tmp_2Yb$), **2**, with neutral bis(methyliminophosphoranyl)-pyridine ligands ($\mathbf{L^R}$) in which the steric demand was modulated at the phosphorus position. These syntheses gave us the opportunity to gather information on the geometric modulation of the Tmp and Cp* ligands when the steric bulk of the equatorial ligand increases, a study that is relevant to the elucidation of the sterically induced reduction in lanthanoids' complexes. The use of the pincer ligands $\mathbf{L^R}$ is rationalized by their ability to act as hemilabile ligands[31] and also by the good σ and π donating ability of iminophosphoranyl ligands that suits well with rare earth metal ions.[32-35] Herein, the solid-state structures of the complexes are reported along with their solution dynamic behaviour. The latter studies highlight the evolution of the $^1J_{Yb\text{-}P}$ coupling constant in agreement with the modification of the coordination mode of the Tmp ligand.

## RESULTS AND DISCUSSION

**Syntheses and Solid-state Crystal Structures.** The ligands $\mathbf{L^{Et}}$ and $\mathbf{L^{Cy}}$ were synthesized in high yield according to the published synthesis[31] of $\mathbf{L^{Ph}}$ from the 2,6-bis(azidomethyl)pyridine and the corresponding phosphines $PEt_3$ and $PCy_3$. $\mathbf{L^{Et}}$ and $\mathbf{L^{Cy}}$ show a singlet in $^{31}P\{^1H\}$ NMR at 25.6 ppm and 20.5 ppm (thf-$d_8$), respectively, which compares well with the singlet resonance observed at 9.9 ppm (in $CD_2Cl_2$) for $\mathbf{L^{Ph}}$. All the ligands are moisture sensitive and are kept in the glovebox.

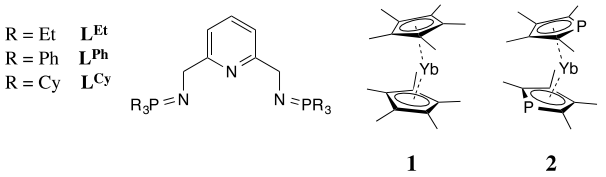


**Figure 1.** Representation of the ligands used in this work, $\mathbf{L^{Et}}$, $\mathbf{L^{Cy}}$ and $\mathbf{L^{Ph}}$ and of the divalent fragments $Cp^*_2Yb$ (**1**) and $Tmp_2Yb$ (**2**).

X-Ray suitable crystals of $\mathbf{L^{Ph}}$ and $\mathbf{L^{Cy}}$ are obtained by recrytallization from concentrated toluene solutions and ORTEP are shown in Figure 2 while main structural parameters are in ESI. The ligands crystalize in their unfolded form with an alternation of the N(2)-C(7)-N(3)-C(6)-N(1) atoms in zigzag. The P(2)-P(1) distance is maximized and is 10.04 Å and 9.84 Å in $\mathbf{L^{Ph}}$ and $\mathbf{L^{Cy}}$, respectively. The mean free N-P distance of the iminophosphoranyl groups is 1.55(1) Å and 1.57(1) Å in $\mathbf{L^{Ph}}$ and $\mathbf{L^{Cy}}$, respectively. The N-C distance of the nitrogen of the iminophosphoranyl group and the carbon next to it is 1.45(1) Å for $\mathbf{L^{Ph}}$ and 1.450(3) Å for $\mathbf{L^{Cy}}$. The C-C and C-N pyridine distances are 1.38(1) Å 1.340(3) Å for $\mathbf{L^{Ph}}$ and 1.385(5) Å 1.34(1) Å for $\mathbf{L^{Cy}}$ in agreement with an aromatic pyridine. Space-fill views shows that the steric hindrance tends to be a little more important in $\mathbf{L^{Cy}}$ than in $\mathbf{L^{Ph}}$ but differences are minimal between these two ligands (See ESI).

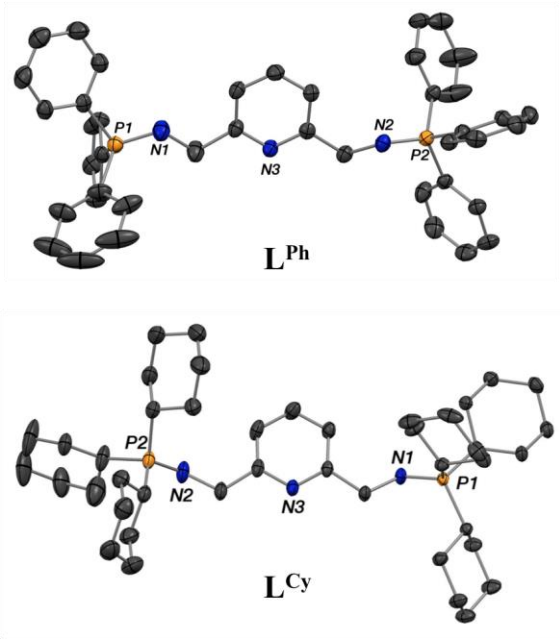


**Figure 2.** ORTEP of $\mathbf{L^{Ph}}$ and of $\mathbf{L^{Cy}}$. Ellipsoids are represented at 50 % level. Carbon atoms are in dark grey, phosphorus atoms in orange and nitrogen atoms in blue. Hydrogen atoms are removed for clarity.

The reaction of $Cp^*_2Yb(OEt_2)$[36,37] with $\mathbf{L^{Et}}$ is performed in diethylether and leads to a deep green solution from which green X-Ray suitable crystals of $Cp^*_2Yb\mathbf{L^{Et}}$ (**1-L$^{Et}$**) are obtained in good yield by letting stand the solution at room temperature. The reaction of $Cp^*_2Yb(OEt_2)$ with $\mathbf{L^{Ph}}$ is also performed in diethylether but the solubility of the resulting complex $Cp^*_2Yb\mathbf{L^{Ph}}$ (**1-L$^{Ph}$**) is lower and a silver-colored powder is obtained in good yield after 1 h of stirring. The latter can be recrystallized in toluene, yielding dark green X-Ray suitable crystals of **1-L$^{Ph}$**. The reaction of **1** with $\mathbf{L^{Cy}}$ was also attempted and monitored by $^{31}P\{^1H\}$ NMR spectroscopy but no sign of the eventual coordination of $\mathbf{L^{Cy}}$ is observed after several hours and only **1** can be recrystallized from the reaction mixture.

The X-Ray crystal structure of **1-L$^{Et}$** and **1-L$^{Ph}$** are shown in Figure 3 and metrical parameters are found in Table 1 and in ESI. The structure of **1-L$^{Et}$** shows the $\kappa^2$ coordination of $\mathbf{L^{Et}}$ to the ytterbium metal center with the nitrogen atom of the pyridine (2.562(3) Å) and a nitrogen atom of an iminophosphoranyl group (2.511(3) Å) while the other is not coordinated. The mean Cp*(C)-Yb distance of 2.77 Å is slightly longer than that found in $Cp^*_2Yb(py)_2$[38] and $Cp^*_2Yb(thf)$[36] of 2.74 Å and 2.66 Å, respectively, and are therefore in agreement with the divalent nature of the ytterbium metal center in **1-L$^{Et}$** (*N.B.* the mean Cp*-Yb distance is 2.50(1) Å). The pyridine C-C and C-N distances are uniform and are of 1.385(7) Å and 1.353(2) Å, respectively, which do not indicated any eventual electron transfer. The C-N and N-P bond distances of the iminophosphoranyl arm coordinated to the ytterbium metal center are 1.480(8) Å and 1.593(3) Å, respectively and are slightly longer than in the non-coordinated arm (1.444(7) Å and 1.561(4) Å). Similar distances and differences between coordinated and free N-P were found in the copper bromide complex with $\mathbf{L^{Ph}}$ and are in agreement with a strong σ donation at the nitrogen atom that removes charge density from the nearest bonds.[31]

| | **1-L$^{Et}$** | **1-L$^{Ph}$** | **2-L$^{Et}$** | **2-L$^{Ph}$** | **2-L$^{Cy}$** | **3** |
|---|---|---|---|---|---|---|
| Yb-Ctr ($\eta^5$-centroid) | 2.50(1) | 2.42(1) | 2.573 | 2.586(1) | 2.614 | 2.51(2) |
| Yb-N(py) | 2.562(3) | 2.53(1) | 2.493(2) | 2.562(2) | 1.466(3) | 2.517(3) |
| Yb-N(iminophosphorane) | 2.511(3) | - | 2.52(1) | 2.556(2) | 2.60(1) | - |
| Ctr-Yb-Ctr | 136 | 140 | 123 | 133 | 111 | 137 |

**Table 1.** Main structural parameters, for **1-L$^{Et}$**, **1-L$^{Ph}$**, **2-L$^{Et}$**, **2-L$^{Ph}$**, **2-L$^{Cy}$** and **3**. Distances are in Å and angles in °. Ctr is for centroid.

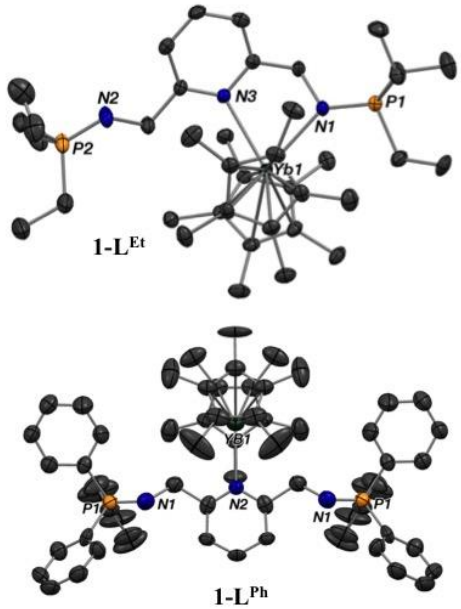


**Figure 3.** ORTEP of **1-L$^{Et}$** and of **1-L$^{Ph}$**. Ellipsoid are represented at 50 % level. Carbon atoms are in dark grey, phosphorus atoms in orange, nitrogen atoms in blue and ytterbium atoms in green. Hydrogen atoms and co-crystallized solvent molecules are removed for clarity.

Replacing the ethyl groups by phenyl groups modified greatly the coordination mode of **L$^{R}$**. The X-ray crystal structure of **1-L$^{Ph}$** shows a $\kappa^1$ coordination mode for the ligand (**L$^{Ph}$**) by the nitrogen atom of the pyridine while the two N=PPh$_3$ moieties are flanked on both side of the Cp*$_2$Yb fragment and remain not coordinated. The N-P distance of 1.562(8) Å is close to that observed in non-coordinated groups and confirmed the above statement. The mean Yb-C(Cp) distance is 2.65 Å and is 0.11 Å shorter than that of **1-L$^{Et}$**. This can be explained by the decrease of the coordination number and a less constrained structure at the ytterbium metal center. Finally the Yb-N(pyridine) distance (Yb-N(3)) is 2.53(1) Å, that is only slightly shorter than that of **1-L$^{Et}$** (2.562(3) Å).

The different coordination modes found in the crystal structures of **1-L$^{Et}$** and **1-L$^{Ph}$** can be explained by the different steric hindrance caused by the presence of larger phenyl groups instead of ethyl groups. However, this may be taken cautiously because additional effects of the solid-state bulk, packing and stacking effects may also contribute to this result since the solid-state structure of **1-L$^{Ph}$** contains two highly disordered toluene molecules (See ESI). Furthermore, the solution properties of these both complexes will give the beginning of an answer and is presented later in the manuscript.

Complexes **2-L$^{Et}$**, **2-L$^{Ph}$** and **2-L$^{Cy}$** are synthesized in diethylether combining Tmp$_2$Yb(thf)[39] and the ligands **L$^{Et}$**, **L$^{Ph}$** and **L$^{Cy}$**, respectively, at room temperature. While **2-L$^{Ph}$** and **2-L$^{Cy}$** are obtained as green powders in good yield, **2-L$^{Et}$** is obtained as a sticky solid and trituration in pentane is necessary to obtain a clean green powder in moderate yield. Green X-ray suitable crystals can be obtained for all three complexes, from diffusion of pentane onto a concentrated toluene solution of **2-L$^{Et}$**, by letting stand a concentrated toluene/methylcyclohexane solution of **2-L$^{Ph}$** at -40 °C and by letting stand a concentrated toluene/pentane solution of **2-L$^{Cy}$** at -40 °C. ORTEP of these crystals structures are shown in Figure 5 and main distances and parameters in Table 1 and ESI. The divalent ytterbium complex Tmp$_2$Yb(py)$_2$ (**3**) was also prepared from Tmp$_2$Yb(thf)$_2$[40] in order to obtain X-ray quality crystals for structural comparison with **2-L$^{Et}$**, **2-L$^{Ph}$** and **2-L$^{Cy}$**. An ORTEP of **3** is shown in Figure 4.

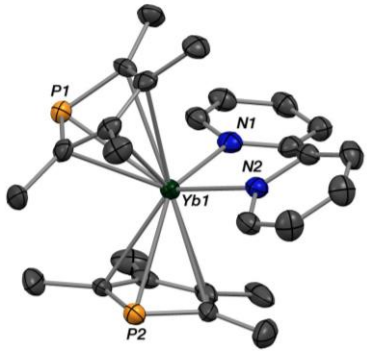


**Figure 4.** ORTEP of **3**. Ellipsoid are represented at 50 % level. Carbon atoms are in dark grey, phosphorus atoms in orange, nitrogen atoms in blue and ytterbium in green. Hydrogen atoms are removed for clarity.

Complex **3** shows two coordinated pyridine molecules and two $\eta^5$-tetramethylphospholyl ligands. The mean Yb-N distance is 2.517(3) Å and the Yb-P and Yb-C(Tmp) distances are 2.94(2) Å and 2.81(3) Å, respectively, while the Yb-Tmp centroid distance is 2.51(2) Å and the Tmp-Yb-Tmp angle is 137 °. The two Tmp ligands are eclipsed and the phosphorus atoms are found in the opposite side to that of the pyridine.

The X-Ray crystal structure of **2-L$^{Et}$** is surprising in the sense that the coordination mode is different that than of **1-L$^{Et}$** although the sterics of Cp* and Tmp present minimal differences. **2-L$^{Et}$** shows a pincer coordination mode in $\kappa^3$ for **L$^{Et}$** while one of the Tmp ligand is coordinated with an $\eta^1$ hapticity and the second remain in $\eta^5$ mode. This behavior is likely to be due to the electronic difference between Tmp and Cp* ligands, the former being less electron donating than the latter, and is very interesting since it shows that the steric pressure of the equatorial ligand may induce a coordination switch of the Tmp ligand. Several other lanthanides complexes with such a coordination mode are known (see Chart 1) but only two in the divalent state. The Yb-N(3) distance is 2.493(2) Å, that is 0.02 Å shorter than that found in **3** and 0.04 Å and 0.06 Å shorter than these of **1-L$^{Et}$** and **1-L$^{Ph}$**, respectively. The Yb-N mean distance of the two iminophosphoranyl moieties is 2.52(1) Å, that is in the same range than that of the coordinated one in **1-L$^{Et}$**. The Yb-Tmp centroid distance found for the $\eta^5$ Tmp ligand is of 2.573 Å and is 0.06 Å longer compared to **3**. This is likely to be

due to the steric bulk provided by the $\mathbf{L^{Et}}$ ligand. Finally the Yb-P(4) distance of the $\eta^1$ coordinated Tmp ligand is 2.9723(8) Å. This is relatively long compared to the $Cp^*_2Sm(C_4Me_4P)$ complex (Chart 1), in which the Sm-P distances are 2.856(1) Å and 2.891(1) Å (two molecules in the unit cell).[30] This shows well how the metal center is sterically constrained because of the pincer coordination type of $\mathbf{L^{Et}}$. The better chelation (entropic effect) of $\mathbf{L^{Et}}$ in a pincer mode ($\kappa^3$) compared to the $\eta^5$ coordination mode of Tmp ligand is likely to contribute to the $\eta^1$ hapticity switch of one Tmp ligand. However, the pure entropic origin of this effect is to take cautiously (pure steric) because the entropy gain of the Tmp ligand switch is not known. Moreover, because this switch is not observed in $\mathbf{1\text{-}L^{Et}}$, it also indicates that the σ- coordination enthalpy (compared to that of the $\eta^5$ mode) of the Tmp ligand plays a sizeable role in this result. Larger groups than ethyl were necessary to get insights in these questions.

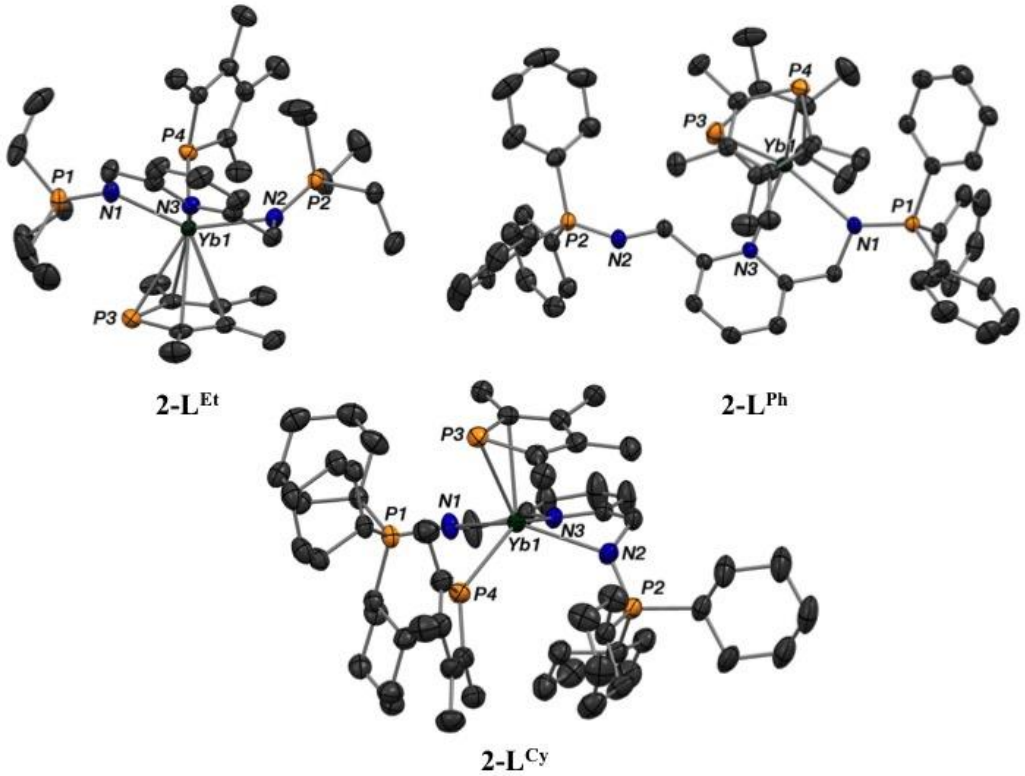


**Figure 5.** ORTEP of $\mathbf{2\text{-}L^{Et}}$, of $\mathbf{2\text{-}L^{Ph}}$ and $\mathbf{2\text{-}L^{Cy}}$. Carbon atoms are in dark grey, phosphorus atoms in orange, nitrogen atoms in blue and ytterbium atom in green. Ellipsoids are represented at 50 % level. Hydrogen atoms and co-crystallized solvent molecules are removed for clarity.

Replacing the ethyl groups by bulkier phenyl or cyclohexyl groups, the solid-state data show two different outcomes for the complexes $\mathbf{2\text{-}L^{Ph}}$ and $\mathbf{2\text{-}L^{Et}}$. $\mathbf{2\text{-}L^{Cy}}$ presents a similar structure than that of $\mathbf{2\text{-}L^{Et}}$ with the ligand $\mathbf{L^{Et}}$ coordinated in a pincer mode, one of the Tmp ligand in $\eta^5$ hapticity and the other one in $\eta^1$ (Figure 5). The mean Yb-N distance of the two iminophosphoranyl moieties is 2.60(1) Å, which is 0.08 Å longer compared to $\mathbf{2\text{-}L^{Et}}$. This significant elongation of the coordination distances of $\mathbf{L^{Cy}}$ with Yb is not reflected by the Yb-N(3) distance that is decreased to 1.466(3) Å. This can be explained by the steric hindrance of the cyclohexyl groups that leads to an increased distance between to the two arms (N(1)-N(2) distance of 4.65 Å in $\mathbf{2\text{-}L^{Cy}}$ compared to 4.55 Å in $\mathbf{2\text{-}L^{Et}}$). However, in order to accommodate the charge density at the metal center, a mechanical decrease of the Yb-N(3) bond is induced with a concomitant slight increase of the N(1)N(2)N(3) bite angle (112° for 2-$L^{Et}$ and 114° in 2-$L^{Cy}$. The Yb-Tmp distance of the centroid to the ytterbium is 2.614 Å, that is 0.04 Å longer compared to the distance found in $\mathbf{2\text{-}L^{Et}}$, and the Yb-P(4) distance is 3.023 Å, again 0.04 Å longer than that of $\mathbf{2\text{-}L^{Et}}$. Finally, the angles between the plane formed by the $\eta^1$ Tmp ligand and the mean plane formed by all atoms of the pincer ligands $\mathbf{2\text{-}L^{Et}}$ and $\mathbf{2\text{-}L^{Cy}}$ are 78 and 86 °, respectively. The latter measurement is a good indication of the $\eta^1$ switch of the Tmp ligand and shows well it is almost perpendicular to the equatorial ligand in $\mathbf{2\text{-}L^{Cy}}$.

Phenyl groups are larger than ethyl groups but the steric demand at the metal center of a coordinated N=$PPh_3$ moiety is almost comparable than that of coordinated N=$PCy_3$ groups. However, the crystal structure of $\mathbf{2\text{-}L^{Ph}}$ presents a different arrangement than the one found in $\mathbf{2\text{-}L^{Et}}$ and $\mathbf{2\text{-}L^{Cy}}$ (Figure 4). The structure is similar to that of $\mathbf{1\text{-}L^{Et}}$ with two phospholyl ligands coordinated in $\eta^5$ and the $\mathbf{L^{Ph}}$ ligand coordinated in $\kappa^2$ with the coordination of the nitrogen atom of the pyridine and the nitrogen atom of one of the two iminophosphoranyl groups. The Yb-N(1) distance is 2.556(2) Å and is longer than that found in $\mathbf{1\text{-}L^{Et}}$ (2.511(3) Å) and is intermediate between those of $\mathbf{2\text{-}L^{Et}}$ and $\mathbf{2\text{-}L^{Cy}}$. The Yb-N(3) distance is 2.562(2) Å and is longer than these found for $\mathbf{2\text{-}L^{Et}}$ and $\mathbf{2\text{-}L^{Cy}}$ because of the different coordination mode but comparable to that of $\mathbf{1\text{-}L^{Et}}$ that exhibits the same coordination mode. The Yb-Tmp distance is 2.586(1) Å, which shows a significant increase compared to **3** in agreement with an increase of the steric bulk on the phosphorus atoms, but is intermediate between the ($\eta^5$-Tmp)-Yb distances of $\mathbf{2\text{-}L^{Et}}$ and $\mathbf{2\text{-}L^{Cy}}$. Finally the Tmp-Yb-Tmp angle is 133° and is comparable to the one of **3**.

Another relevant measurement for the description of the $\eta^5$-$\eta^1$ switch in these complexes lies in the measurement of the Tmp-Yb-Tmp (centroids) angle. This angle is 137 ° for **3**

and 133° in **2-L$^{Ph}$**, complexes in which solid-state data indicate that the two Tmp ligands are coordinated in $\eta^5$, but shrinks to 123° in **2-L$^{Et}$** and 111° for **2-L$^{Cy}$**, when one of the Tmp ligand switches to $\eta^1$. If the solid-state metrics tend to show that the steric bulk is likely to be the principal reason, it is facilitated with the phospholyl group since the σ- coordination is possible compared to the bonding situation of the Cp* group. In this set of five structures, two features are noticeable. The first concern the Cp* series and lies in the $\kappa^1$ coordination of the **L$^{Ph}$** ligand. As it is discussed above, it is likely that the phenyl group may engage in stacking interactions with solvent molecules or with the phenyl groups of other molecules. These forces - that are typically around few kcal,[41] may be strong enough, if additive, to disfavour the $\kappa^2$ coordination in the solid state as it is observed for **1-L$^{Et}$**. In the Tmp series, the **L$^{Ph}$** ligand also behaves differently than **L$^{Et}$** and **L$^{Cy}$** although the steric hindrance is very similar between phenyl groups and cyclohexyl groups. The rigidity of the phenyl moieties may explain this result as well as the reduced Lewis basicity of the **L$^{Ph}$** ligand compared to the **L$^{Et}$** and **L$^{Cy}$** ligands. Because the sole solid-state data cannot confirm these hypotheses in solution, the solution dynamic behavior of all these five complexes was studied and is presented in the next paragraph.

**Solution Properties.** The dissolution of **1-L$^{Et}$** and **1-L$^{Ph}$** in a thf-$d_8$ solution led to only one singlet resonance in $^{31}P\{^1H\}$ NMR observed at 33.8 ppm and 14.7 ppm, respectively. The $^1H$ NMR data also show five resonances for the **L$^{Et}$** ligand and six resonances for the **L$^{Ph}$** ligand. Additionally, one Cp* resonance is present in both cases at 2.06 ppm and 2.08 ppm, respectively. These data are in agreement with a $C_{2v}$ symmetry in solution, a different situation than that found in the crystals structure of **1-L$^{Et}$**. Decreasing the temperature of the thf-$d_8$ solution of **1-L$^{Et}$** leads to a decrease in intensity of the phosphorus resonance at around -40 °C and to two well separated signals at -80 °C. One resonance is found at 29.4 ppm, a value that is very close to that found for the free ligand in thf-$d_8$ ($\delta_P$ = 25.6 ppm), and the other is found at 40.4 ppm and is attributed to the coordinated arm. This signal presents also additional satellites that are attributed to the $^2J_{Yb\text{-}P}$ coupling with a value of 55.0 Hz, a value comparable to that obtained by Roesky *et al.* in their iminophosphoranyl complexes of divalent ytterbium.[42] This situation (at -80 °C) is in good agreement to that found in the solid-state and that was described above. Taken together, these data are in agreement with a fast dynamic exchange of the two iminophosphoranyl arms in solution, as shown in Scheme 1. This behaviour was also reported for copper complexes with **L$^{Ph}$** and shows nicely the hemilability of **L$^{Et}$**.

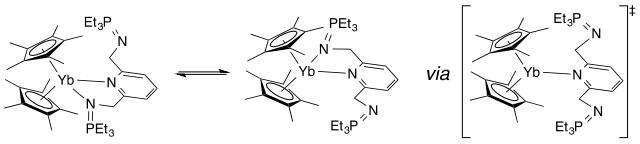


**Scheme 1.**

The same variable temperature experiment was performed with a solution of **1-L$^{Ph}$** and also leads to the decoalescence of the sole resonance found in $^{31}P\{^1H\}$ NMR at around -80 °C to form two new resonances at 31.9 and 9.2 ppm. This is more surprising since it indicates a different situation than the one found in the crystal structure of **1-L$^{Ph}$**. The analysis of the coalescence signal shape with the temperature leads to the activation parameters of the exchange process which are $\Delta H^‡$ = 15.7(2) kcal.mol$^{-1}$ and $\Delta S^‡$ = 24(1) cal.mol$^{-1}$.K$^{-1}$, for **1-L$^{Et}$** and $\Delta H^‡$ = 7.9(3) kcal.mol$^{-1}$ and $\Delta S^‡$ = - 0.7(5) cal.mol$^{-1}$.K$^{-1}$ for **1-L$^{Ph}$**. The value of $\Delta H^‡$ for **1-L$^{Et}$** is significantly higher than that found in the copper complex CuBrL$^{Ph}$ (7.3(1) kcal.mol$^{-1}$)[31] and is in agreement with a larger steric bulk induced by the Cp* ligands. The large positive $\Delta S^‡$ suggests that the mechanism is dissociative since large positive entropy is in agreement with a transition state that is less organized than the reactant and the product. A complex, in which the two iminophosphoranyl groups are dissociated, is likely to resemble the transition state (Scheme 1). This situation is different than that found in CuBr**L$^{Ph}$**, for which an interchange mechanism is reported.[31]

The situation of **1-L$^{Ph}$** is a little different. A large decrease of the activation entropy is observed in comparison to **1-L$^{Et}$**, and it shrinks to a similar value than that obtained for the copper complex CuBrL$^{Ph}$ although the steric bulk is amply larger in **1-L$^{Ph}$**. The activation entropy value is close to zero and is not in agreement with a dissociative mechanism. Form these data, it is clear that the exchange mechanism is different in the two complexes **1-L$^{Et}$** and **1-L$^{Ph}$**. A small entropic barrier implies that the shape of the transition state is close to the one of the product. The X-ray crystal structure of **1-L$^{Ph}$** suggests that the form in which the two arms are not coordinated (unfolded structure, **I**) is stabilized enough and a two steps mechanism in which **I** is not a transition state is likely to happen. The shape of the transition state is therefore closer to the reactant shape, that has only one arm coordinated and exhibits a lower activation enthalpy than that of **1-L$^{Et}$** because the dissociation of the second arm is facilitated by the formation of **I**. Lowering the temperature to -90 °C did not allow the observation of the postulated intermediate **I** in solution.

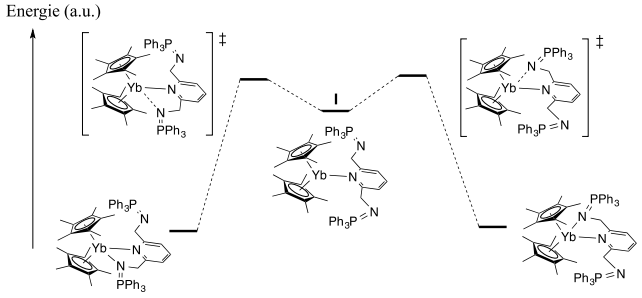


**Scheme 2.**

The reasons for the stabilization of the dissociated form of **1-L$^{Ph}$** are not obvious and could be the addition of a large steric bulk and of weak intermolecular interactions in solution. The fact that **L$^{Cy}$** does not react with the Cp*$_2$Yb fragment would suggest that the steric hindrance plays a major role in the solution behavior of **1-L$^{Ph}$**.

From the X-ray data and the solution dynamic data, it seems that the Cp* ligands remain coordinated in $\eta^5$ and do not switch to $\eta^1$ when the steric bulk is increased in the equatorial position. However, if this switch is dynamical, only the average symmetry is retained and this is the reason why we choose to replace the Cp* ligand by a Tmp ligand. In the latter, a σ coordination is possible at the phosphorus center and the Tmp ligand possesses a similar steric hindrance than the Cp* ligand. The elongated C-P distance in the cycle partially compensates the absence of one methyl in the ring. Moreover, the mean Yb-C distance is longer because of the presence of the bigger phosphorus atom as exemplified by the mean Yb-C distance of 2.81(3) Å found in **3** compared to 2.74(1) Å found in Cp*$_2$Yb(py)$_2$.

When crystals of **2-L$^{Ph}$** are dissolved in toluene-$d_8$, three different resonances are present in $^{31}P\{^1H\}$ NMR at 79.0 ppm, 20.3 ppm and 5.8 ppm. The resonance at 79.0 ppm exhibits

two satellites separated by a coupling constant of 172.3 Hz that is attributed to the $^{1}J_{Yb\text{-}P}$ coupling and the resonance is therefore attributed to the phosphorus of the Tmp ligand. The two other resonances are attributed to a coordinated iminophosphoranyl group and a non-coordinated one. This $C_s$ symmetry in solution indicates a similar situation to that found in the solid state with two phospholyl ligands coordinated in $\eta^5$ and the $\mathbf{L^{Ph}}$ ligand coordinated in $\kappa^2$ by the pyridine and one arm of the N=PPh$_3$ group (Scheme 3). Interestingly, it shows that the two arms are not in exchange like it was discussed above for **1-L$^{Ph}$** and **1-L$^{Et}$**.

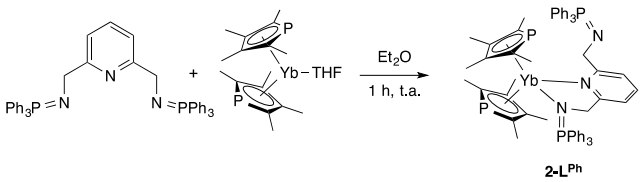


**Scheme 3.**

The $^{1}J_{Yb\text{-}P}$ is rather large compared to the one observed in **3** that is of 105.5 Hz. This may not be ascribed to the Yb-P distance, which is similar in both complexes (2.94(2) Å in **3** and 2.947(1) Å in **1-L$^{Ph}$**), but rather to the coordination angle of the phosphorus atom to the ytterbium metal. The three main mechanisms in the scalar coupling (or indirect coupling) are the spin-orbit contribution (diamagnetic and paramagnetic), the spin-dipole contribution and the Fermi contact.[43] For the $^{31}$P atom, the principal contributions are the Fermi contact and the paramagnetic spin-orbit contribution. The Fermi contact is directly related to the relative s contribution in the observed atom and is therefore related to the σ bonding scheme[44] of the Tmp ligand. On the other hand, the paramagnetic spin-orbit contribution is related to the π orbitals.[45,46] The increase of the $^{1}J_{Yb\text{-}P}$ is therefore related to the bonding mode of the phosphorus atom in the Tmp ligand. The NMR of **2-L$^{Et}$** and **2-L$^{Cy}$** is then of high importance to test this conjecture because of the observed $\eta^1$ coordination mode as described above in the X-ray structures.

The $^{31}$P{$^{1}$H} NMR spectra of **2-L$^{Et}$** and **2-L$^{Cy}$** performed in toluene-d$^8$ shows two resonances at room temperature at 77.9 ppm and 47.2 ppm for **2-L$^{Et}$** and at 79.3 ppm and 38.8 ppm for **2-L$^{Cy}$**. The presence of $^{2}J_{Yb\text{-}P}$ coupling constants of 42.9 Hz and 47.0 Hz for **2-L$^{Et}$** and **2-L$^{Cy}$**, respectively and the symmetry of the complex in solution indicate the coordination of both the iminophosphoranyl arms at room temperature, which is markedly different from **1-L$^{Et}$**, in which an exchange is observed. The presence of a sole resonance for the Tmp ligand is in agreement with an average symmetry between the two ligands and could be in agreement with either a $\eta^5$ coordination of both Tmp ligand or a dynamic $\eta^5$-$\eta^1$ switch but that is faster than the NMR time scale (Scheme 4). Lowering the temperature did not lead to a splitting of the corresponding resonances of **L$^{Et}$** and **L$^{Cy}$** but the resonances attributed to the Tmp ligand split at around -90 °C to give two resonances at 81.6 ppm and 70.0 ppm for **2-L$^{Et}$** and at 84.4 ppm and 76.8 ppm for **2-L$^{Cy}$**. The broadness of the signal did not allow determining the individual $^{1}J_{Yb\text{-}P}$ coupling. The analysis of the shape of the resonances at the coalescence temperature allows the determination of the activation parameters that are $\Delta H^{\ddagger}$ = 7.4(3) kcal.mol$^{-1}$ and $\Delta S^{\ddagger}$ = -3.5(5) cal.mol$^{-1}$.K$^{-1}$, for **2-L$^{Et}$** and $\Delta H^{\ddagger}$ = 9.8(3) kcal.mol$^{-1}$ and $\Delta S^{\ddagger}$ = 2.8(5) cal.mol$^{-1}$.K$^{-1}$ for **2-L$^{Cy}$**. The increase of the activation enthalpy in **2-L$^{Cy}$** is in good agreement with the increased bulk of the **L$^{Cy}$** ligand compared to **L$^{Et}$**. The two activation entropy values are close to zero and seem in good agreement with a concerted inter-conversion (Scheme 4).[47,48]

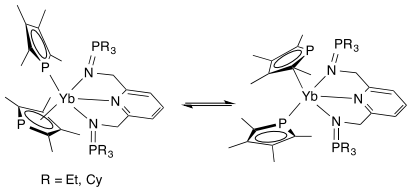


**Scheme 4.**

The $^{1}J_{Yb\text{-}P}$ values are 434.7 Hz and 491.4 Hz for **2-L$^{Et}$** and **2-L$^{Cy}$**, respectively, and are very large compared to those reported for **3** and **2-L$^{Ph}$** (Figure 6). Such an increase is in excellent agreement with the $\eta^1$ coordination of one of the Tmp ligand and a fast dynamic of the two Tmp ligands in solution (see Scheme 4). The σ-coordination mode of the Tmp ligand leads to an increased s character of the bonding, which amplifies the Fermi contact contribution and the absolute value of the indirect coupling. Such large $^{1}J_{Yb\text{-}P}$ were already reported in phosphine[49] and phosphide complexes of ytterbium,[50-56] in which the ligand is coordinated in a $\eta^1$-σ fashion. The increase of this value from **2-L$^{Et}$** and **2-L$^{Cy}$** also correlates well to the structural parameters difference noted in the previous section such as the angle between the plane of the equatorial ligands, **L$^{Et}$** and **L$^{Cy}$**, and the Tmp ligand or the Tmp-Yb-Tmp angle. A clear trend can be drawn between the $^{1}J_{Yb\text{-}P}$ values and the situation found in the X-ray crystal structures.

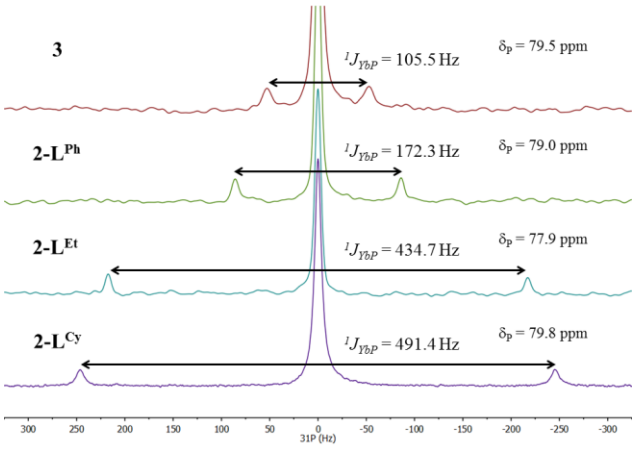


**Figure 6.** Comparison of the $^{1}J_{Yb\text{-}P}$ values obtained from $^{31}$P{$^{1}$H} NMR in toluene-d$_8$ at room temperature for **3**, **2-L$^{Ph}$**, **2-L$^{Et}$** and **2-L$^{Cy}$**.

This observation is very important since it gives a tool to follow the destabilization of the Tmp ligand that is relevant for the study of sterically induced reduction.[17] In these reactions, the $\eta^5$-$\eta^1$ switch is postulated to be at the origin of this singular reactivity.[57] If sterically induced reduction reactions are often reported with Cp* ligands and samarium, some of us recently showed that phospholyl ligands complexes of the smaller thulium cation may behave the same way.[19] The complexes described in this work push away our knowledge of the coordination chemistry of Cp* and phospholyl ligands with lanthanides, greatly helped by the NMR $^{1}J_{Yb\text{-}P}$ coupling constants.

## CONCLUSION

In conclusion, we report the synthesis, the X-ray structure and the dynamic solution behaviour of ytterbocene and phosphaytterbocene fragments with neutral pincer bis(iminophosphoranyl) ligands. The main feature of these complexes is that the Tmp ligand can switch to a $\eta^1$ coordination mode when

the steric bulk increases while this is not observed for the Cp* ligand. The modification of the coordination mode can be followed in solution by monitoring the $^{1}J_{Yb\text{-}P}$ coupling constants in the phospholyl complexes. The coupling constant increases dramatically when a ligand is coordinated in $\eta^1$ because of the increased Fermi contact derived from a σ-coordination although the symmetry remain high in solution because of the fast dynamic switch of the two Tmp ligands. This observation is reinforced with the solid-sate data that are in good agreement with the solution behavior. Because the $\eta^5$-$\eta^1$ switch is relevant for the study of the sterically induced reduction reactions in lanthanides, we hope to take advantage of this tool to gain insights in the mechanism of this reaction and discover novel reactivity with ytterbium since it was only reported for samarium, thulium and uranium complexes. Work in this direction is currently in progress.

## EXPERIMENTAL SECTION

**General considerations.** All reactions were conducted under an atmosphere of dry nitrogen, or argon, using standard Schlenk and glovebox techniques. Solvents and reagents were obtained from commercial sources. Tetrahydrofuran, pentane, dichloromethane, diethyl ether, toluene and petroleum ether were dried with an MBraun MB-SPS 800 solvent purification system (for ligand syntheses) or over sodium/benzophenone (for reaction with divalent ytterbium). $CD_3CN$ was distilled from $CaH_2$, under dry nitrogen, other deuterated solvents were used as received and stored over molecular sieves. 2,6-bis(azidomethyl)pyridine and $\mathbf{L^{Ph}}$,[31] $Cp^*_2Yb(OEt_2)$ (**1-OEt₂**)[29] and $Tmp_2Yb(thf)$ (**1-thf**)[30] (**2**) were prepared following literature procedure.

Nuclear magnetic resonance (NMR) spectra were recorded on a Bruker Av300 spectrometer operating at 300 MHz for $^{1}H$, 75.5 MHz for $^{13}C$, and 121.5 MHz for $^{31}P$. Solvent peaks were used as internal references for $^{1}H$ and $^{13}C$ chemical shifts (ppm). $^{31}P$ peaks were referenced to external 85% $H_3PO_4$. The following abbreviations are used; br, broad; s, singlet; d, doublet; t, triplet; m, multiplet; hept, heptuplet, bd; fr, free, bonded. Labelling of atoms is indicated in Scheme 5. Elemental analyses were from the London Metropolitan University.

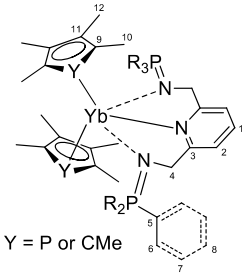


**Scheme 5.**

**Syntheses. Synthesis of $\mathbf{L^{Et}}$.** To a Schlenk flask containing 2,6-bis(azidomethyl)pyridine (5.45 mmol, 1.03 g), a solution of $PEt_3$ (2 equiv., 1.29 g, 10.9 mmol in 10 mL of petroleum ether) was slowly added via cannula (about 15 min.). The reaction induced a strong nitrogen evolution (the flask should be open, under nitrogen flux) and turned pink. The mixture was stirred for an extra hour. A singlet at 23.6 ppm in $^{31}P$ NMR indicated the completion of the reaction. Solvents were evaporated under reduced pressure, yielding a slightly pink powder, which was sonicated and dried again under vacuum. Upon standing the pink color (maybe caused by traces of the phosphazide) disappears to yield 1.29 g of $\mathbf{L^{Et}}$ (94%).

$^{31}P\{^{1}H\}$ NMR (THF-$d^8$) δ 25.6 (s). $^{1}H$ NMR (THF-$d^8$) δ 7.43 (s, 3H, $H_{1+2}$, $H_1$ and $H_2$ are magnetically equivalent, confirmed by HSQC), 4.22 (d, $^{3}J_{PH}$ = 19.7 Hz, 4H, $H_4$), 1.64 (dq, $^{2}J_{PH}$ = 11.5 Hz, $^{3}J_{HH}$ = 7.7 Hz, 12H, $H_5$), 1.64 (dt, $^{3}J_{PH}$ = 15.3 Hz, $^{3}J_{HH}$ = 7.7 Hz, 18H, $H_6$). $^{13}C$ NMR (THF-$d^8$) δ 165.8 (d, $J$ = 17.9 Hz, $C_3$), 135.6 ($C_1$), 118.2 ($C_2$), 52.1 (d, $J_{PC}$ = 4.5 Hz, $C_4$), 19.2 (d, $J_{PC}$ = 62.2 Hz, $C_5$), 6.5 (d, $J_{PC}$ = 4.5 Hz, $C_6$). Calcd for $C_{19}H_{37}N_3P_2$: C, 61.77; H, 10.09; N, 11.37. Found: C, 61.64; H, 10.15; N, 11.47.

**Synthesis of $\mathbf{L^{Cy}}$.** To a Schlenk flask containing 2,6-bis(azidomethyl)pyridine (5.71 mmol, 1.08 g) in $Et_2O$ (20 mL), a solution of $PCy_3$ (2.1 equiv., 1.29 g, 12.0 mmol) in 50 mL of $Et_2O$ and THF (v/v 4:1) was added via cannula. Evolution of nitrogen was not obvious but the colour changed to pink. The phosphazide intermediate was detected ($\delta_P$ = 33.0 ppm).[58] The reaction was stirred under a stream of nitrogen for 3 h., then closed and stirred overnight at room temperature. A white precipitate was formed and completion of the reaction was checked by NMR showing a broad singlet at 20.8 ppm in $^{31}P\{^{1}H\}$ NMR and traces of $PCy_3$ (9.0 ppm) and $OPCy_3$ (45.0 ppm). The solvent volume was reduced to about 20 mL. The solution was filtered under nitrogen and washed with petroleum ether (20 mL) to yield a white solid that was dried under high *vacuum* for 3 h (3.22 g, 4.64 mmol). The filtrate was kept at -78°C for 1 h to induce the crystallization of another crop of solid (0.65 g). In total, $\mathbf{L^{Cy}}$ was obtained in 93 % yield. $^{31}P\{^{1}H\}$ NMR ($C_6D_6$) δ 20.5 (s). $^{1}H$ NMR ($C_6D_6$) δ 8.22 (d, $^{3}J_{HH}$ = 7.6 Hz, 2H, $H_2$), 7.75 (t, $^{3}J_{HH}$ = 7.6 Hz, 1H, $H_1$), 5.06 (d, $^{3}J_{PH}$ = 14.2 Hz, 4H, $H_4$), 2.19-0.84 (m, 66H, $H_{5+6+7+8}$). $^{13}C$ ($C_6D_6$) δ 166.3 (d, $J_{PC}$ = 20.5 Hz, $C_3$), 136.2 ($C_1$), 118.5 ($C_2$), 53.0 (d, $J_{PC}$ = 4.0 Hz, $C_4$), 35.8 (d, $J_{PC}$ = 57.5 Hz, $C_5$), 27.8 (d, $J_{PC}$ = 6.5 Hz, $C_6$), 27.7 (d, $J_{PC}$ = 14.5 Hz, $C_7$), 26.8 (s, $C_8$). Calcd for $C_{43}H_{73}N_3P_2$: C, 74.42; H, 10.60; N, 6.05. Found: C, 74.36; H, 10.77; N, 6.15. The compound was also univocally identified by X-ray analysis of crystals obtained by recrystallization of the petroleum ether layer (see Figure 2 and ESI, S2).

**Synthesis of $\mathbf{Cp^*_2YbL^{Et}}$ ($\mathbf{1\text{-}L^{Et}}$).** In a glove-box, **1-OEt₂** (15.9 mg, 30.7 µmol) and $\mathbf{L^{Et}}$ (11.4 mg, 30.8 µmol) were mixed in $Et_2O$ (1.5 mL) leading to the formation of a deep green solution which was stirred for 10 minutes. After stopping the stirring and upon standing for few extra minutes, crystals appeared; the mixture was allowed to stand at - 40°C overnight leading to the formation of green crystalline blocks. After filtration, the crystals were washed with pentane (1.5 mL) and dried under reduce pressure for 1 h to yield $\mathbf{1\text{-}L^{Et}}$ (17.3 mg, 66%). $^{31}P\{^{1}H\}$ NMR (THF-$d^8$, 35°C) δ 33.8 (brs). $^{1}H$ NMR (THF-$d^8$, 35°C) δ 7.60 (brt, 1H, $H_1$), 7.51 (brd, 2H, $H_2$), 4.29 (brd, $^{3}J_{PH}$ *ca.* 12 Hz, 4H, $H_4$), 2.06 (brs, 30H, $H_{10}$), 1.69 (brdq, 12H, $H_5$), 1.05 (brdt, $^{2}J_{PH}$ *ca.* 15 Hz, $^{3}J_{HH}$ *ca.* 8 Hz, 18H, $H_6$). $^{13}C\{^{31}P\}$ NMR (THF-$d^8$, 35°C) δ 138.0 ($C_1$), 124.3 ($C_2$), 111.5 ($C_9$), 52.3 ($C_4$), 19.6 ($C_5$), 12.7 ($C_{10}$), 7.3 ($C_6$), $C_3$ was not observed. Calcd for $C_{39}H_{67}N_3P_2Yb$: C, 57.62; H, 8.31; N, 5.17. Found: C, 57.55; H, 8.39; N, 5.20. Suitable crystals for X-Ray analysis were obtained by standing for 2 h. a concentrated solution in $Et_2O$ at room temperature.

**Synthesis of $\mathbf{Cp^*_2YbL^{Ph}}$ ($\mathbf{1\text{-}L^{Ph}}$).** In a glove box, $\mathbf{L^{Ph}}$ (69.1 mg, 105.0 µmol) and **1-OEt₂** (54.4 mg, 105 µmol) were mixed in $Et_2O$ (4 mL) and stirred for 1 h leading to the formation of a green precipitate. The mixture was filtered and the solid washed with $Et_2O$ (2 mL) and pentane (2x3 mL). Finally the dark green solid was dried under high *vacuum* for 2 h to yield $\mathbf{1\text{-}L^{Ph}}$ as a silver-coloured powder (96 mg, 87 µmol, 83 %). $^{31}P\{^{1}H\}$ NMR ($C_6D_6$) δ 14.7 (s). $^{1}H$ NMR ($C_6D_6$) δ 7.97 (d, $^{3}J_{HH}$ = 7.7 Hz, 2H, $H_2$), 7.87-7.68 (m, 18H, $H_{6+8}$), 7.62 (t, $^{3}J_{HH}$ = 7.7 Hz, 1H, $H_1$), 7.13-6.97 (m, 12H, $H_7$), 4.49 (d, $^{3}J_{PH}$ = 14.9 Hz, 4H, $H_4$), 2.08 (s, 30H, $H_{10}$). $^{13}C$ NMR ($C_6D_6$) δ 164.7 (d, $J_{PC}$ = 24.0 Hz, $C_3$), 137.5 (s, $C_1$), 133.3 (d, $J_{PC}$ = 95.7 Hz, $C_5$), 133.1 (d, $J_{PC}$ = 9.1 Hz, $C_6$), 131.7 (d, $J_{PC}$ = 3.2 Hz, $C_8$), 128.8 (d, $J_{PC}$ = 11.6 Hz, $C_7$), 120.8 (s, $C_2$), 112.3 (s, $C_9$), 50.4 (s, $C_4$), 12.0 (s, $C_{10}$). Calcd for $C_{63}H_{67}N_3P_2Yb$: C, 68.71; H, 6.13; N, 3.82. Found: C, 66.62; H, 6.32; N, 3.92. Suitable crystals for X-Ray analysis were obtained by cooling a concentrated toluene solution at -40 °C.

**Synthesis of $\mathbf{Tmp_2YbL^{Et}}$ ($\mathbf{2\text{-}L^{Et}}$).** $Et_2O$ (10 mL) was condensed to a flask containing $\mathbf{L^{Et}}$ (140.9 mg, 0.38 mmol) and **1-THF** (200.0 mg, 0.38 mmol), the mixture was then stirred at room temperature for 1 h. resulting in the formation of a green sticky solid. The $Et_2O$ was removed and pentane (5 mL) was added, the mixture was triturated with a spatula and stirred for another 30 minutes allowing the formation of a dark green solid. The solid was isolated by filtration and dried under high *vacuum* to yield $\mathbf{2\text{-}L^{Et}}$ as a dark green solid (226.1 mg, 0.275 mmol, 72%).

$^{31}P\{^{1}H\}$ NMR (Tol-$d^8$) δ 77.9 (s, $^{1}J_{YbP}$ = 434.7 Hz), 47.2 (s, $^{2}J_{YbP}$ = 42.9 Hz). $^{1}H$ NMR (Tol-$d^8$) δ 7.10 (t, $^{3}J_{HH}$ = 7.5 Hz, 1H, $H_1$), 6.47 (d, $^{3}J_{HH}$ = 7.5 Hz, 2H, $H_2$), 4.13 (d, $^{3}J_{PH}$ = 14.6 Hz, 4H, $H_4$), 2.45 (d, $^{2}J_{PH}$ = 10.5 Hz, 12H, $H_{10}$), 2.22 (s, 12H, $H_{12}$), 1.70 (dq, $^{2}J_{PH}$ = 12.9 Hz, $^{3}J_{HH}$ = 7.6 Hz, 12H, $H_5$), 0.78 (dt, $^{3}J_{PH}$ = 15.5 Hz, $^{3}J_{HH}$ = 7.6 Hz, 18H, $H_6$). $^{13}C$ NMR ($CD_3CN$) δ 163.2 (d,

$J_{PC}$ = 21.7 Hz, $C_3$), 138.5 (s, $C_1$), 120.6 (s, $C_2$), 52.2 (s, $C_4$), 17.5 (d, $J_{PC}$ = 61.2 Hz, $C_5$), 16.2 (d, $J_{PC}$ = 31.4 Hz, $C_{10}$), 14.0 (s, $C_{12}$), 6.9 (d, $J_{PC}$ = 4.4 Hz, $C_6$), $C_9$ and $C_{11}$ were not observed. Calcd for $C_{35}H_{61}N_3P_4Yb$: C, 51.21; H, 7.49; N, 5.12. Found: C, 51.35; H, 7.55; N, 5.22. Suitable crystals for X-Ray analysis were obtained by diffusion of pentane onto a concentrated solution in toluene.

**Synthesis of $Tmp_2YbL^{Ph}$ ($2\text{-}L^{Ph}$).** In a centrifugation tube, $L^{Ph}$ (75.2 mg, 0.11 mmol) and **1-THF** (60 mg, 0.11 mmol) were stirred in $Et_2O$ (3 mL) for 1 h. leading to the formation of a green precipitate. Pentane (5 mL) was added to enhance the precipitation and the mixture was centrifuged. The supernatant was removed and the solid washed with pentane (5 mL) in the same manner, the solid was finally dried under high *vacuum* to yield $\mathbf{2\text{-}L^{Ph}}$ (104.5 mg, 82%). $^{31}P\{^1H\}$ NMR (Tol-$d^8$) δ 79.0 (s, $^1J_{Yb\text{-}P}$ = 172.3 Hz), 20.3 (s, bd N=P), 5.8 (s, fr N=P). $^1H$ NMR (Tol-$d^8$) δ 8.15 (d, $^3J_{HH}$ = 7.4 Hz, 1H, $H_{2,bd/2,fr}$), 7.89-7.67 (m, *ca.* 16H, $H_{Ar}$), 7.41-6.88 (m, *ca.* 16H, $H_{Ar}$), 4.78 (d, $^3J_{PH}$ = 16.2 Hz, 2H, $H_{4,bd}$, 4.56 (d, $^3J_{PH}$ = 15.9 Hz, 2H, $H_{4,fr}$), 2.30 (d, $^2J_{PH}$ = 10.1 Hz, 12H, $H_{10}$), 1.97 (s, 12H, $H_{12}$). The moderate solubility in THF-$d^8$ and $C_6D_6$ prevents meaningful $^{13}C$ analysis. Elemental analysis, Calcd. for $C_{59}H_{61}N_3P_4Yb$: C, 63.89; H, 5.54; N, 3.79. Found: C, 63.84; H, 5.64; N, 3.65. Suitable crystals for X-Ray analysis were obtained by letting stand a concentrated toluene/methylcyclohexane solution of the compound at -40 °C.

**Synthesis of $Tmp_2YbL^{Cy}$ ($2\text{-}L^{Cy}$).** In a centrifugation tube, $L^{Cy}$ (127 mg, 0.18 mmol) and [Yb(tmp)$_2$(THF)] (96 mg, 0.18 mmol) were stirred in $Et_2O$ (2 mL) for 3 h leading to the formation of a green precipitate. Pentane (10 mL) was added to enhance the precipitation and the mixture was centrifuged and stored at – 40 °C overnight. The liquid was removed and the operation repeated another time with 10 mL of pentane. Finally the dark green solid was dried under high *vacuum* for 2 h. to yield $\mathbf{2\text{-}L^{Cy}}$ (130 mg, 0.11 mmol, 62 %). $^{31}P\{^1H\}$ NMR (Tol-$d^8$) δ 79.8 (s, $^1J_{YbP}$ = 491.4 Hz), 38.8 (s, $^2J_{YbP}$ = 47.0 Hz). $^1H$ NMR ($C_6D_6$) δ 7.42-7.33 (m, 3H, $H_{1+2}$), 4.70 (d, $^3J_{PH}$ = 14.8 Hz, 4H, $H_4$), 2.58 (d, $^2J_{PH}$ = 10.6 Hz, 12H, $H_{10}$), 2.39 (s, 12H, $H_{12}$), 2.27-0.99 (m, 66H, $H_{5+6+7+8}$). $^{13}C$ NMR ($C_6D_6$) δ 165.6 (d, $J_{PC}$ = 15.8 Hz, $C_3$), 138.0 (s, $C_1$), 135.1 (d, $J_{PC}$ = 28.8 Hz, $C_9$), 129.4 (s, $C_{11}$), 119.7 (s, $C_2$), 51.0 (s, $C_4$), 35.2 (d, $J_{PC}$ = 56.2 Hz, $C_5$), 27.8 (d, $J_{PC}$ = 3.1 Hz, $C_6$), 27.3 (d, $J_{PC}$ = 11.3 Hz, $C_7$), 26.5 (s, $C_8$), 16.7 (d, $J_{PC}$ = 27.3 Hz, $C_{10}$), 14.9 (s, $C_{12}$). Elemental analysis, Calcd. for C59H97N3P4Yb: C, 61.87; H, 8.54; N, 3.67. Found: C, 61.63; H, 8.62; N, 3.65. Suitable crystals for X-Ray analysis were obtained by standing a concentrated toluene/pentane solution of the compound at -40 °C.

**X-Ray Diffraction.** Single crystals of the compounds $\mathbf{L^{Ph}}$, $\mathbf{L^{Cy}}$, $\mathbf{1\text{-}L^{Et}}$, $\mathbf{1\text{-}L^{Ph}}$, $\mathbf{2\text{-}L^{Et}}$, $\mathbf{2\text{-}L^{Ph}}$, $\mathbf{2\text{-}L^{Cy}}$ and **3** were mounted on a kapton loop using Paratone® oil and cooled to 150 K in a nitrogen stream for X-ray structure determination. The loop was transferred to a Nonius Kappa diffractometer using Mo-Kα (λ = 0.71073 Å) X-ray source, a graphite monochromator and a Brucker APEX-II detector. Preliminary orientation matrixes and cell constants were determined by collection of 10x10 s frames, followed by spot integration and least-squares refinement. Data were integrated and corrected for Lorentz and polarization effects. The crystal structures were solved in SIR97[59] and refined in SHELXL-2013[60] by full-matrix least-squares using anisotropic thermal displacement parameters for all non-hydrogen atoms. All hydrogen atoms were placed at geometrically calculated positions. Details on crystal data and structure refinements are summarized in Table S1. ORTEP drawings were produced using Mercury or ORTEP III for Windows.

Cif files were deposited at the Cambridge Data Base Centre under the reference CCDC numbers: 1423768 ($\mathbf{L^{Ph}}$), 1423769 ($\mathbf{L^{Cy}}$), 1423770 ($\mathbf{1\text{-}L^{Et}}$), 1423771 ($\mathbf{1\text{-}L^{Ph}}$), 1423772 (**3**), 1423773 ($\mathbf{2\text{-}L^{Et}}$), 1423774 ($\mathbf{2\text{-}L^{Ph}}$) and 1423775 ($\mathbf{2\text{-}L^{Cy}}$).

**Supporting Information**. Information concerning X-ray crystallography and variable temperature NMR is available.

## AUTHOR INFORMATON

### Corresponding Authors

greg.nocton@polytechnique.edu (G.N.), audrey.auffrant@polytechnique.edu (AA)

**Notes**

The authors declare no competing financial interest

## ACKNOWLEDGMENT

We thank CNRS and Ecole Polytechnique for financial support, Prof. Dr. Richard A. Andersen and Dr. François Nief for many scientific discussions and help. TC thanks Ecole polytechnique for PhD fellowship.

## REFERENCES

(1) Szostak, M.; Procter, D. J. *Angew. Chem. Int. Ed.* **2012**, *51*, 9238.
(2) Evans, W. J. *J. Alloy. and Compd.* **2009**, *488*, 493.
(3) Evans, W. J. *Coord. Chem. Rev.* **2000**, *206*, 263.
(4) Nief, F. *Dalton Trans.* **2010**, *39*, 6589.
(5) Szostak, M.; Spain, M.; Procter, D. J. *Chem. Eur. J.* **2014**, *20*, 4222.
(6) Evans, W. J.; Rego, D. B.; Ziller, J. W.; DiPasquale, A. G.; Rheingold, A. L. *Organometallics* **2007**, *26*, 4737.
(7) Jaroschik, F.; Nief, F.; Le Goff, X. F.; Ricard, L. *Organometallics* **2007**, *26*, 3552.
(8) Labouille, S.; Nief, F.; Le Goff, X.-F.; Maron, L.; Kindra, D. R.; Houghton, H. L.; Ziler, J. W.; Evans, W. J. *Organometallics* **2012**, *31*, 5196.
(9) Nocton, G.; Lukens, W. L.; Booth, C. H.; Rozenel, S. S.; Melding, S. A.; Maron, L.; Andersen, R. A. *J. Am. Chem. Soc.* **2014**, *136*, 8626.
(10) Nocton, G.; Ricard, L. *Chem. Commun.* **2015**, *51*, 3578.
(11) Nocton, G.; Booth, C. H.; Maron, L.; Andersen, R. A. *Organometallics* **2013**, *32*, 1150.
(12) Nocton, G.; Ricard, L. *Dalton Trans.* **2014**, *43*, 4380.
(13) Andrez, J.; Pécaut, J.; Bayle, P.-A.; Mazzanti, M. *Angew. Chem. Int. Ed.* **2014**, *53*, 10448.
(14) Zitz, R.; Hlina, J.; Gatterer, K.; Marschner, C.; Szilvasi, T.; Baumgartner, J. *Inorg. Chem.* **2015,** *54*, 7065.
(15) Andrez, J.; Bozoklu, G.; Nocton, G.; Pecaut, J.; Scopelliti, R.; Dubois, L.; Mazzanti, M. *Chem. Eur. J.* **2015**, *DOI: 10.1002/chem.201502204*.
(16) Ruspic, C.; Moss, J. R.; Schürmann, M.; Harder, S. *Angew. Chem. Int. Ed.* **2008**, *47*, 2121.
(17) Evans, W. J. *J. Organomet. Chem.* **2002**, *647*, 2.
(18) Evans, W. J.; Forrestal, K. J.; Ziller, J. W. *J. Am. Chem. Soc.* **1998**, *120*, 9273.
(19) Jacquot, L.; Xémard, M.; Clavaguéra, C.; Nocton, G. *Organometallics* **2014**, *33*, 4100.
(20) Evans, W. J.; Miller, K. A.; Lee, D. S.; Ziller, J. W. *Inorg. Chem.* **2005**, *44*, 4326.
(21) Miller, K. L.; Williams, B. N.; Benitez, D.; Carver, C. T., Ogilby, K. R.; Tkatchouk, E.; Goddard, W. A. III.; Diaconescu, P. L. *J. Am. Chem. Soc.* **2010**, *132*, 342.
(22) Gornitzka, H.; Steiner, A.; Stalke, D.; Kilimann, U.; Edelmann, F. T. *J. Organomet. Chem.* **1992**, *439*, C6.
(23) Carver, C. T.; Benitez, D.; Miller, K. L.; Williams, B. N.; Tkatchouk, E.; Goddard, W. A. III.; Diaconescu, P. L. *J. Am. Chem. Soc.* **2009**, *131*, 10269.
(24) Huang, W.; Carver, C. T.; Diaconescu, P. L. *Inorg. Chem.* **2011**, *50*, 978.
(25) Butovskii, M. V.; Tok, O. L.; Bezugly, V.; Wagner, F. R.; Kempe, R. *Angew. Chem. Int. Ed.* **2011**, *50*, 95.
(26) Bauer, T.; Wagner, F. R.; Kempe, R. *Chem. Eur. J.* **2013**, *19*, 8732.
(27) Sobaczynski, A. P.; Bauer, T.; Kempe, R. *Organometallics* **2013**, *32*, 1363.
(28) Butovskii, M. V.; Dörjing, C.; Bezugly, V.; Wagner, F. R.; Grin, Y.; Kempe, R. *Nature Chem.* **2010**, 2, 741.
(29) Nief, F.; Ricard, L. *J. Organomet. Chem.* **1994**, *464*, 149.

(30) Nief, F.; Ricard, L. *Organometallics* **2001**, *20*, 3884.
(31) Cheisson, T.; Auffrant, A. *Dalton Trans.* **2014**, *43*, 13399.
(32) Bakewell, C.; Cao, T.-P.-A.; Long, N.; Le Goff, X. F.; Auffrant, A.; Williams, C. K. *J. Am. Chem. Soc.* **2012**, *134*, 20577.
(33) Rong, W.; Cheng, J.; Mou, Z.; Xie, H.; Cui, D., *Organometallics* **2013,** *32*, 5523-5529.
(34) Gamer, M. T.; Roesky, P. W., *Inorg. Chem.* **2004,** *43*, 4903-4906.
(35) Martinez-Arripe, E.; Jean-Baptiste-dit-Dominique, F.; Auffrant, A.; Le Goff, X. F.; Thuilliez, J.; Nief, F., *Organometallics* **2012,** *31*, 4854-4861.
(36) Tilley, T. D.; Andersen, R. A.; Spencer, B.; Ruben, H.; Zalkin, A.; Templeton, D. H. *Inorg. Chem.* **1980**, *19*, 2999.
(37) Tilley, T. D.; Boncella, J. M.; Berg, D. J.; Burns, C. J.; Andersen, R. A.; Lawless, G. A.; Edelman, M. A.; Lappert, M. F. In *Inorg. Syn.*; John Wiley & Sons, Inc.: 2007, p 146.
(38) Tilley, T. D.; Andersen, R. A.; Spencer, B.; Zalkin, A. *Inorg. Chem.* **1982**, *21*, 2647.
(39) Nief, F.; Ricard, L.; Mathey, F. *Polyhedron* **1993**, *12*, 19.
(40) Nief, F.; Mathey, F. *Synlett* **1991**, 745.
(41) Wagner, J. P.; Schreiner, P. R. *Angew. Chem. Int. Ed.* **2015**, *DOI: 10.1002/anie.201503476*
(42) Schmid, M.; Ona-Burgos, P.; Guillaume, S. M.; Roesky, P. W. *Dalton Trans.* **2015**, *44*, 12338.
(43) Ramsey, N. F. *Phys. Rev.* **1953**, *91*, 303.
(44) Wu, A.; Gräfenstein, J. R.; Cremer, D. *J. Phys. Chem. A* **2003**, *107*, 7043.
(45) Gräfenstein, J. R.; Cremer, D. *Chem. Phys. Lett.* **2004**, *383*, 332.
(46) Cremer, D.; Kraka, E.; Wu, A.; Lüttke, W. *ChemPhysChem* **2004**, *5*, 349.
(47) Merbach, A. E. *Pure App. Chem.* **1982**, *54*, 1479.
(48) Merbach, A. E. *Pure App. Chem.* **1987**, *59*, 161.
(49) Fryzuk, M. D.; Haddad, T. S.; Berg, D. J. *Coord. Chem. Rev.* **1990**, *99*, 137.
(50) Basalov, I. V.; Lyubov, D. M.; Fukin, G. K.; Cherkasov, A. V.; Trifonov, A. A. *Organometallics* **2013**, *32*, 1507.
(51) Karsch, H. H.; Ferazin, G.; Kooijman, H.; Steigelmann, O.; Schier, A.; Bissinger, P.; Hiller, W. *J. Organomet. Chem.* **1994**, *482*, 151.
(52) Rabe, G. W.; Riede, J. r.; Schier, A. *Inorg. Chem.* **1996**, *35*, 40.
(53) Rabe, G. W.; Yap, G. P. A.; Rheingold, A. L. *Inorg. Chem.* **1997**, *36*, 3212.
(54) Rabe, G. W.; Guzei, I. A.; Rheingold, A. L. *Inorg. Chem.* **1997**, *36*, 4914.
(55) Clegg, W.; Izod, K.; Liddle, S. T.; O'Shaughness, P.; Sheffield, J. M. *Organometallics* **2000**, *19*, 2090.
(56) Izod, K.; O'Shaughnessy, P.; Sheffield, J. M.; Clegg, W.; Liddle, S. T. *Inorg. Chem.* **2000**, *39*, 4741.
(57) Evans, W. J.; Perotti, J. M.; Kozimor, S. A.; Champagne, T. M.; Davis, B. L.; Nyce, G. W.; Fujimoto, C. H.; Clark, R. D.; Johnston, M. A.; Ziller, J. W. *Organometallics* **2005**, *24*, 3916.
(58) Fortman, G. C.; Captain, B.; Hoff, C. D. *Inorg. Chem.* **2009**, *48*, 1808.
(59) Altomare, A.; Burla, M. C.; Camalli, M.; Cascarano, G. L.; Giacovazzo, C.; Guagliardi, A.; Moliterni, A. G. G.; Polidori, G.; Spagna, R. *J. App. Cryst.* **1999**, *32*, 115.
(60) Sheldrick, G. *Acta Cryst. A* **2008**, *64*, 112.